The Astrophysical Journal, 652:1768–1781, 2006 December 1


# THE PHYSICS OF PROTOPLANETESIMAL DUST AGGLOMERATES. I. MECHANICAL PROPERTIES AND RELATIONS TO PRIMITIVE BODIES IN THE SOLAR SYSTEM

Jürgen Blum and Rainer Schräpler
Institute for Geophysics and Extraterrestrial Physics, Technical University at Braunschweig, Mendelssohnstr. 3, D-38106 Braunschweig, Germany; j.blum@tu-bs.de

Björn J. R. Davidsson
Department of Astronomy and Space Physics, Uppsala University, Box 515, SE-75120 Uppsala, Sweden; bjorn.davidsson@astro.uu.se

and

Josep M. Trigo-Rodríguez
Institut de Ciènces de l'Espai (CSIC), Campus UAB, Facultat de Ciènces, Torre C-5, parells, 2a planta, E-08193 Bellaterra (Barcelona), Spain; and Institut d'Estudis Espacials de Catalunya (IEEC), Ed. Nexus, Gran Capità 2-4, E-08034 Barcelona, Spain; trigo@ieec.uab.es
*Received 2006 June 27; accepted 2006 July 26*

## ABSTRACT

We present laboratory experiments on the formation of macroscopic dust aggregates. The centimeter-sized highly porous bodies are produced by random ballistic deposition from individual micrometer-sized dust particles. We find packing densities between 0.07 and 0.15 for uncompressed samples, dependent on the shape and size distribution of the constituent dust grains. Impacts into these bodies are simulated by uniaxial compression experiments. We find that the maximum compression, equivalent to the highest protoplanetary impact velocities of $\sim$50 m s$^{-1}$, increases the packing density to 0.20–0.33. Tensile strength measurements with our laboratory samples yield values in the range 200–1100 Pa for slightly compressed samples. We review packing densities and tensile strengths found for primitive solar system bodies, e.g., for comets, primitive meteorites, and meteoroids. We find a consistency between packing densities and tensile strengths of our laboratory samples with those from cometary origin.

*Subject headings:* dust, extinction — methods: laboratory — planetary systems: formation — solar system: formation

*Online Material:* color figures

## 1. INTRODUCTION

In the commonly considered formation scenario for planetesimals, these kilometer-sized planetary precursors form due to nonelastic collisions between dust agglomerates in combination with adhesive surface forces. Weidenschilling & Cuzzi (1993) and Weidenschilling (1997) have outlined the general theoretical picture of planetesimal and cometesimal formation, in which the preplanetary dust grains initially—when the collision velocities are caused by Brownian motion and differential drift motions, and are thus very moderate— coagulate into fractal dust agglomerates. Subsequently, when the mutual impact energies become sufficiently high due to higher drift velocities, sticking collisions result in nonfractal dust agglomerates.

In a series of experimental papers, this theoretical model was basically confirmed and refined. Heim et al. (1999) showed that the contact forces between micron-sized $SiO_2$ grains were indeed of the previously assumed van der Waals type. Poppe et al. (2000a) measured the sticking properties in single-grain collisions for various particle shapes, materials, and sizes and found that spherical grains possess a well-defined sticking threshold of typically a few m s$^{-1}$, whereas irregular grains are better characterized by a sticking probability, which is typically a few $\times$ 10% for collision velocities above 1 m s$^{-1}$. Blum et al. (2000, 1998), Wurm & Blum (1998), and Krause & Blum (2004) performed aggregation experiments with dust clouds in rarefied gases, in which the collisions were caused by Brownian motion (Blum et al. 2000; Krause & Blum 2004), differential sedimentation (Blum et al. 1998), and gas turbulence (Wurm & Blum 1998), respectively. In all those agglomeration scenarios, the collision velocities were well below 1 m s$^{-1}$, and fractal dust aggregates formed very rapidly. A fractal dust agglomerate is characterized by a mass-size relation in which the mass of a dust agglomerate $m$ scales with its characteristic size $s$, following a power law of the form $m \propto s^{D_f}$. Here the exponent $D_f$ is the fractal dimension, which typically obtains values of $D_f < 2$. A general finding was that the mass distribution of dust aggregates in low-velocity agglomeration experiments is always rather narrow (quasi-monodisperse) so that, at a given time, predominantly dust clusters of similar mass and size are present. This behavior was also found in the theoretical investigations by Weidenschilling & Cuzzi (1993) and Weidenschilling (1997), and can be understood using Smoluchowski's coagulation equation (Smoluchowski 1916) with a ballistic kernel and fractal particles (Blum 2006).

Ballistic impact experiments of fractal dust clusters show a transition from fractal to nonfractal growth when the impact energy exceeds the rolling-friction threshold (Blum & Wurm 2000). Agglomerate fragmentation is observed for impact velocities above a few m s$^{-1}$. Both findings are in quantitative agreement with the numerical agglomerate collision model by Dominik & Tielens (1997) when the experimental values for the threshold energies for particle break-up (Poppe et al. 2000a) and rolling friction (Heim et al. 1999) are taken into account (see, Blum & Wurm 2000).

By comparing the results of these models and experiments with the physical properties of primitive solar system objects, we can improve our knowledge of the initial stage of planetesimal formation in the solar nebula. The modeling results show that

within a few hundred to several tens of thousands of years (depending on the radial distance from the Sun), the largest fractal aggregates form due to Brownian motion and, thereafter, due to differential settling of the agglomerates toward the midplane of the preplanetary accretion disk. The aggregate sizes at that stage vary from a few cm at 1 AU to $\sim$100 $\mu$m at 30 AU (Blum 2004). As the agglomerate masses increase, the impact energies exceed the agglomerate restructuring threshold, and subsequent sticking collisions among the dust agglomerates lead to a compaction of the dust aggregates. The sticking probabilities in mutual collisions remain close to unity as long as the fragmentation threshold is not reached. Thus, nonfractal dust agglomerates start to grow. Due to a decreasing surface-to-mass ratio, the collision velocities caused by differential sedimentation increase linearly with the agglomerate sizes. The fragmentation limit is finally reached when the agglomerates have grown to sizes of typically a few cm at 1 AU and roughly 1 mm in the 10–30 AU regime (Blum 2004).

While the first growth steps of protoplanetary bodies are rather simple and straightforward, the processes leading from decimeter to kilometer sizes are still not understood. Due to the higher collision velocities among the dust agglomerates, compaction and fragmentation will be the dominating outcomes in mutual collisions. Experiments by Blum & Münch (1993) have shown that collisions between (almost) equal-sized high-porosity dust agglomerates with collision velocities around 1 m s$^{-1}$ do not lead to further sticking. In contrast, fragmentation dominates the collision outcomes for velocities $\gtrsim$1 m s$^{-1}$. Thus, further growth above the sticking/fragmentation limit (which is somewhat dependent on size and material of the constituent grains in the colliding dust aggregates) is inhibited in such a quasi-monodisperse scenario so that the mass distribution function must be much wider for any further growth to occur.

Another point is worth mentioning and will be addressed in this paper: beyond the limit of aggregate restructuring, the protoplanetary bodies are nonfractal, so that an average mass density for these objects can be defined. However, this mass density is yet unknown. It is obvious that, as long as mutual collisions occur at moderate velocities, the developing dust aggregates can be quite porous. With increasing average collision velocity, we expect that the mass density increases. An increase in density has consequences for the collision velocities because the mass-to-surface ratio, and therefore the gas-grain coupling time, increases. The latter value determines the collision velocities of the grains which typically increase with increasing gas-grain coupling times (Weidenschilling 1977). An increased mass density can also influence the outcome of a collision between dust aggregates: very fluffy aggregates are more likely to stick to one another in low-velocity collisions than compacted dusty bodies (Wurm et al. 2005).

Even though collisions between dust agglomerates might not lead to direct sticking, and might even result in fragmentation or crater formation, further growth of the protoplanetesimals is still feasible under certain conditions. This issue was first addressed by Wurm et al. (2001a, 2001b). Although a considerable fraction of the dust agglomerates might break up in collisions with velocities $\gg$1 m s$^{-1}$, the aerodynamic interaction of the fragments with the ambient gas of the solar nebula can carry the fragments back to the larger of the two colliding bodies. Wurm et al. (2001a, 2001b) experimentally and theoretically showed that an aerodynamic capture of fragments following an impact above the fragmentation limit is in principle feasible. Sekiya & Takeda (2003) argued that the aerodynamic growth stage for protoplanetesimals might be limited to sizes smaller than the mean free path of the embedding gas. These limiting sizes are $\sim$1 cm at 1 AU and $\gtrsim$1 m at 30 AU. Above this size, viscous gas flow around the protoplanetesimals might prevent the fragments from "falling back" onto the larger bodies. However, Wurm et al. (2004) showed that a certain fraction of the fragments, formed in the impact, can still be trapped by the larger body, due to a finite gas permeability of the macroscopic protoplanetary bodies. That picture is consistent with the fact that very primitive meteorites (like carbonaceous chondrites) are formed by fragments of separate bodies (and then called breccias) showing a low degree of compaction. However, these meteorites have experienced some shock heating, inducing compaction, and aqueous alteration (Trigo-Rodríguez et al. 2006). These processes altered the original packing densities of the constituent particles within these porous objects, as we discuss in more detail in § 6.2.

Blum (2004) proposed another mechanism for the growth beyond the fragmentation limit, based on electrostatic charging in mutual collisions. Poppe et al. (2000b) and Poppe & Schräpler (2005) showed that mutual collisions among dust grains lead to an electrostatic charging of the collision partners. A succession of nonsticking collisions between a macroscopic dust agglomerate and smaller bodies in the solar nebula can cause an accumulation of charges on the larger body, whose electrical field close to the surface, as a consequence, grows in strength. At some critical value for the field strength, the escaping fragments, on average oppositely charged to the protoplanetesimal, are no longer able to escape the attractive Coulomb potential and are therefore reattracted to the surface of the larger body. As the mean size of the protoplanetesimals grows, the mean collision velocity, and hence the number of electrostatic charges per unit projectile mass separated in a collision, also increases (Poppe et al. 2000b; Poppe & Schräpler 2005), so that the timescales for reaching the critical electrical field strength decreases. In contrast to the abovementioned "aerodynamic" accretion, we call this phenomenon "electrostatic" accretion.

Weidenschilling & Cuzzi (1993) proposed a runaway growth scenario for the final stage of planetesimal formation, which is qualitatively similar to the "aerodynamic" and "electrostatic" accretion processes. In such a scenario, a few large dust agglomerates grow by accumulation of generally much smaller dust agglomerates. In this paper, we will take a closer look at protoplanetesimals at the stage of runaway growth, regardless of the physical processes behind it. The general questions to be addressed concern the structure and morphology of these bodies as well as their mechanical properties. As Sirono (2004) writes, "Collisional outcomes, such as sticking, cratering or catastrophic disruption, critically depend on the mechanical properties of an aggregate. . . ." Ultimately, we intend to arrive at a better physical description for planetesimals and their potential sole survivors, the comets, as well as a better picture of the collision properties of primitive solid bodies. A first step in this direction is the SPH code developed by Sirono (2004), which is, however, still lacking empirical data of the mechanical properties of low-density dust aggregates. These quantities are required for a model of planetesimal formation, particularly to decide whether runaway growth occurs or not.

In § 2 we elaborate on the theoretical aspects of the morphology of hit-and-stick runaway protoplanetesimals, § 3 deals with the experimental verification of these aspects, and § 4 summarizes the experimental results for packing densities and tensile strengths of macroscopic dust aggregates. In § 5, we draw conclusions about the packing densities and tensile strengths of protoplanetary bodies. Section 6 compiles our knowledge on packing densities and tensile strengths for comets, and meteoritic and meteoroidal material, the bodies closest to planetesimals.

TABLE 1
PHYSICAL PARAMETERS OF THE SPHERICAL $SiO_2$ PARTICLES AND THE IRREGULAR $SiO_2$ AND DIAMOND GRAINS

| Physical Property | Symbol | Value | Unit | Reference |
|---|---|---|---|---|
| | | Spherical $SiO_2$ | | |
| Material | ... | $SiO_2$, non-porous | ... | 1 |
| Morphology | ... | spherical | ... | 1 |
| Molecular arrangement | ... | amorphous | ... | 1 |
| Density | $\rho_0$ | $2.0 \times 10^3$ | kg m$^{-3}$ | 2 |
| Radius | $s_0$ | $0.76 \pm 0.03$ | $\mu$m | 3 |
| Mass | $m_0$ | $(3.7 \pm 0.4) \times 10^{-15}$ | kg | ... |
| Surface molecules | ... | Si-OH | ... | 1 |
| Surface energy | ... | 0.014 | J m$^{-2}$ | 4 |
| Adhesion force | $F_{\rm stick}$ | $(67 \pm 11) \times 10^{-9}$ | N | 4 |
| Adhesion energy | $E_{\rm stick}$ | $(2.2 \pm 0.4) \times 10^{-15}$ | J | 5, 6 |
| Rolling-friction force | $F_{\rm roll}$ | $(0.68 \pm 0.13) \times 10^{-9}$ | N | linear extrapolation from ref. 4 |
| Rolling-friction energy | $E_{\rm roll}$ | $(8.1 \pm 1.9) \times 10^{-16}$ | J | $E_{\rm roll} = F_{\rm roll} \frac{\pi}{2} s_0$ |
| Sticking threshold velocity | $v_{\rm stick}$ | 1.1 | m s$^{-1}$ | extrapolated from ref. 5 |
| Rolling-threshold velocity | $v_{\rm roll}$ | $1.5 \pm 0.3$ | m s$^{-1}$ | $v_{\rm roll} = \sqrt{(10 E_{\rm roll})/m_0}$ |
| | | Irregular diamond | | |
| Material | ... | C, diamond | ... | 7 |
| Morphology | ... | irregular | ... | ... |
| Density | $\rho_0$ | 3520 | kg m$^{-3}$ | ... |
| Size | $s_0$ | $0.75 \pm 0.25$ | $\mu$m | 5 |
| | | Irregular $SiO_2$ | | |
| Material | ... | $SiO_2$, non-porous | ... | 8 |
| Morphology | ... | irregular | ... | ... |
| Density | $\rho_0$ | 2600 | kg m$^{-3}$ | 8 |
| Size | $s_0$ | $\sim$0.05–5 | $\mu$m | 50% of typical particle diameter |

REFERENCES.—(1) Manufacturer information, micromod Partikeltechnologie GmbH; (2) Blum & Schräpler 2004; (3) Poppe & Schräpler 2005; (4) Heim et al. 1999; (5) Poppe et al. 2000a; (6) Blum & Wurm 2000; (7) manufacturer information, Saint-Gobain Diamantwerkzeuge GmbH & Co. KG; (8) manufacturer information, Sigma-Aldrich Chemie GmbH.

In § 7, we try to calculate the tensile strengths of primitive bodies in young solar systems. We briefly conclude our work in § 8 and give an outlook to future activities in § 9.

## 2. THEORETICAL ASPECTS: PACKING DENSITIES OF AGGLOMERATES

The main objective of this paper is to study the mechanical properties of macroscopic protoplanetary dust aggregates. As we do not know the mass densities and internal structures of these bodies, we start with rather low densities and homogeneous bodies and proceed to denser objects by compression experiments. The lowest packing density in dust agglomeration are reached when the ballistically colliding dust aggregates stick to one another at the first point of contact. Any deviation from this hit-and-stick behavior will always result in denser agglomerate configurations. Dominik & Tielens (1997) showed theoretically and Blum & Wurm (2000) confirmed experimentally that for impact energies of the dust particles $E_{\rm imp} < 5E_{\rm roll}$ rolling of the spherical dust grains is inhibited. For the spherical $SiO_2$ grains with radii $s_0 = 0.76$ $\mu$m and mass $m_0 = 3.7 \times 10^{-15}$ kg that we used in our experiments (see Table 1 and § 3), the energy required to roll a dust grain over a quarter of its circumference about another grain is $E_{\rm roll} = 8.1 \times 10^{-16}$ J. Sticking of two spherical grains in collisions will happen for $v_{\rm imp} < v_{\rm stick}$. Thus, for impact velocities $v_{\rm imp} < \min(v_{\rm stick}, v_{\rm roll})$ with $v_{\rm roll} = (10E_{\rm roll}/m_0)^{1/2} = 1.5$ m s$^{-1}$ and $v_{\rm stick} = 1.1$ m s$^{-1}$ (see Table 1), we expect a hit-and-stick behavior. For our experimental $SiO_2$ spheres, we thus get $v_{\rm imp} < 1.1$ m s$^{-1}$. These hit-and-stick impacts result in the lowest packing density, and thus in the highest porosity of the protoplanetesimals.

However, the actual packing density of a growing dust agglomerate is also determined by the morphology of the projectiles from which it is constituted. For individual monomer grains impinging onto a target agglomerate, the packing density will be higher than for projectiles that consist of loose dust aggregates, because the effective volume per unit mass that the projectiles occupy is much higher if the projectiles are open-structured dust aggregates. A process describing the growth of an aggregate by the addition of individual dust grains is the ballistic particle-cluster aggregation (PCA). In terms of early solar system dust mass distribution, PCA refers to a wide or bimodal mass distribution (see § 1). The PCA process results in dust aggregates whose packing densities (i.e., the fraction of volume filled with dust particles) are $\phi = \rho/\rho_0 = 0.15$, and whose porosities are $\pi = 1 - \phi = 0.85$ (Kozasa et al. 1992). Here, $\rho$ and $\rho_0$ are the mass density of the agglomerate and the monomer grain, respectively.

In this paper we concentrate on macroscopic nonfractal dust aggregates formed by a process analogous to the ballistic PCA process, which leads to identical aggregate packing densities, and offers the opportunity of laboratory experiments to reveal their physical properties. This process is termed random ballistic deposition (RBD). In its idealized form, RBD uses individual, spherical, and monodisperse particles, which are deposited randomly but unidirectionally on a semi-infinite target. Numerical simulations with up to $10^6$ particles show that RBD agglomerates have packing densities of $\phi = 0.1469 \pm 0.0004$ (Watson et al. 1997), identical to those of PCA aggregates (Kozasa et al. 1992). Hence, RBD agglomerates have much lower packing densities than the random close-packing (RCP), which is the densest

configuration of randomly arranged monodisperse spherical particles. For RCP, the packing density is $\phi = 0.635$ (see, e.g., Onoda & Liniger 1990; Torquato et al. 2000).

There are two potential causes for a densification of protoplanetesimals: collisional and gravitational compaction, to be discussed in the following.

1. *Compaction by collisions*.— Due to the condition that the original impacts into the protoplanetesimals may exceed the restructuring or fragmentation limit, some compaction of the surface layers will occur. The amount of compaction depends on the mechanical properties of the growing dust agglomerates and on the mass and collision velocities of the projectiles. As a coarse guidance to the pressure that the colliding bodies will experience, let us assume that the impacting body is much smaller than the protoplanetesimal in the runaway growth phase and that the impact energy, which is almost completely used up for restructuring and fragmentation (Sirono 2004), is distributed over roughly twice the impactor's volume. The validity of this assumption will be experimentally confirmed in a forthcoming paper. Hence, if we assume a constant dynamic impact pressure $p_{\rm dyn}$, it will be

$$p_{\rm dyn} \approx \frac{1}{4}\rho v_{\rm imp}^2, \tag{1}$$

where $\rho$ is the mass density of the projectile agglomerate. For $\rho = 1000$ kg m$^{-3}$ and $v_{\rm imp} = 1$–$100$ m s$^{-1}$, we get $p_{\rm dyn} = 2.5 \times 10^2$–$2.5 \times 10^6$ Pa.

2. *Compaction by gravity*.— Larger planetesimals are no longer exclusively bound by attractive surface forces but are partially gravitationally compacted. The central pressure within a homogeneous spherical planetesimal can be expressed by

$$p_c = \frac{2}{3}\pi G \bar{\rho}^2 R^2, \tag{2}$$

where $\bar{\rho}$ and $R$ denote the mean mass density of the planetesimal and the radius of the planetesimal, respectively. However, even for bodies as large as $R = 1$ km, we get maximum central pressures of $p_c \approx 100$ Pa, which is much lower than any impact pressures. Thus, impact compression is the most important process for the densification of protoplanetary dust aggregates with impact pressures ranging from $\sim 10^2$ to $\sim 10^6$ Pa. Our laboratory investigations on aggregate compaction will therefore concentrate on this pressure range.

## 3. EXPERIMENTAL ASPECTS

### 3.1. *Dust Samples*

For the comparison between the numerical studies, models, and the experimental simulations of the runaway growth stage of planetesimal formation, we performed a series of experiments with well-characterized $SiO_2$ grains. These particles are monodisperse, perfectly spherical, have an atomically smooth surface (Heim et al. 1999), and are relevant cosmic dust analogs for the abundant group of silicates. Table 1 summarizes the physical properties of these $SiO_2$ particles. In addition to the spherical $SiO_2$ grains, we also performed experiments with irregularly shaped diamond particles with a narrow size distribution, and with irregular $SiO_2$ grains with a wide size distribution. The properties of these particles are also summarized in Table 1.

With these dust samples, the mechanical properties of three classes of macroscopic dust aggregates can be studied: (1) aggregates consisting of perfectly monodisperse, spherical monomer grains, (2) aggregates consisting of quasi-monodisperse, irregular monomer grains, and (3) aggregates consisting of irregular monomer grains with a wide size distribution. This variety of possible particle properties should enable us to cover the full range of possible monomer size distributions and morphologies.

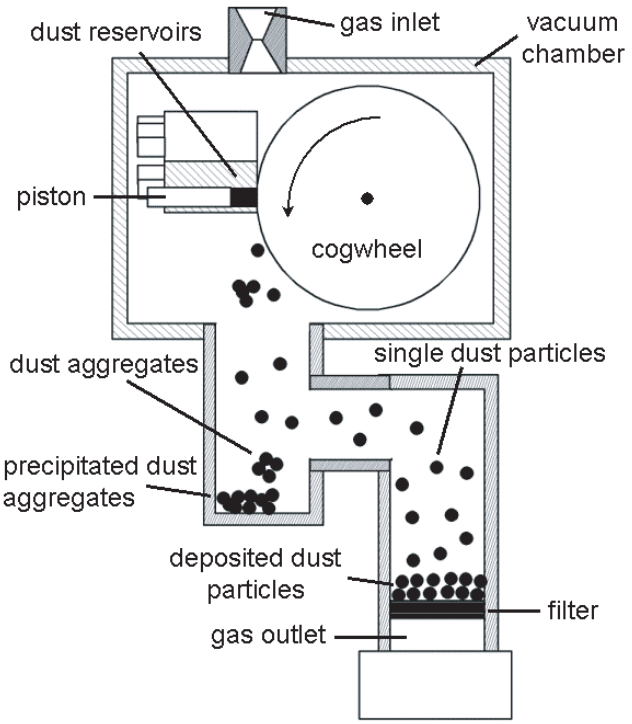


FIG. 1.—Principles of the experimental setup for the formation of macroscopic dust aggregates.

### 3.2. *Experimental Methods*

For the experimental simulation of the RBD process, we developed an experimental setup with which the low-velocity deposition of single, micrometer-sized dust grains in quantities of up to a few grams is feasible. Figure 1 shows the principles of the experimental setup with which we realized a unidirectional hit-and-stick growth of dust aggregates.

The dust sample is filled into 20 dust-reservoir cylinders that are placed in a revolver mechanism. Inside a vacuum chamber, the dust sample is sequentially pushed onto a rotating cogwheel of 100 mm diameter by means of a slowly moving piston. The circumference velocity of the cogwheel is $\sim 15$ m s$^{-1}$, so that the dust sample is deagglomerated into the monomer grains, as described in Poppe et al. (1997). The individual dust particles preferentially leave the cogwheel in the direction of the velocity vector of the cogwheel, and are decelerated in the ambient gas of typically 100 Pa pressure within a stopping distance of $\sim 0.1$ m. Due to a laminar gas flow inside the experimental apparatus, whose velocity is adjusted to a value of $\sim 0.5$ m s$^{-1}$ by a mass-flow controller, the single dust grains are carried along with the gas and are deposited on a thin filter substrate. During the experiment run time of approximately 2 hr, a monolithic dust aggregate of 25 mm diameter and 5–10 mm thickness is formed (see Fig. 2*a*). Thicker dust aggregates can be produced by refilling the dust-reservoir cylinders. The yield of the apparatus, i.e., the ratio of dust mass in the dust aggregate to the total mass of the dust sample prior to deagglomeration, is $\sim 30\%$. The deagglomeration efficiency can be monitored with a long-distance microscope that images the dust grains through an observation

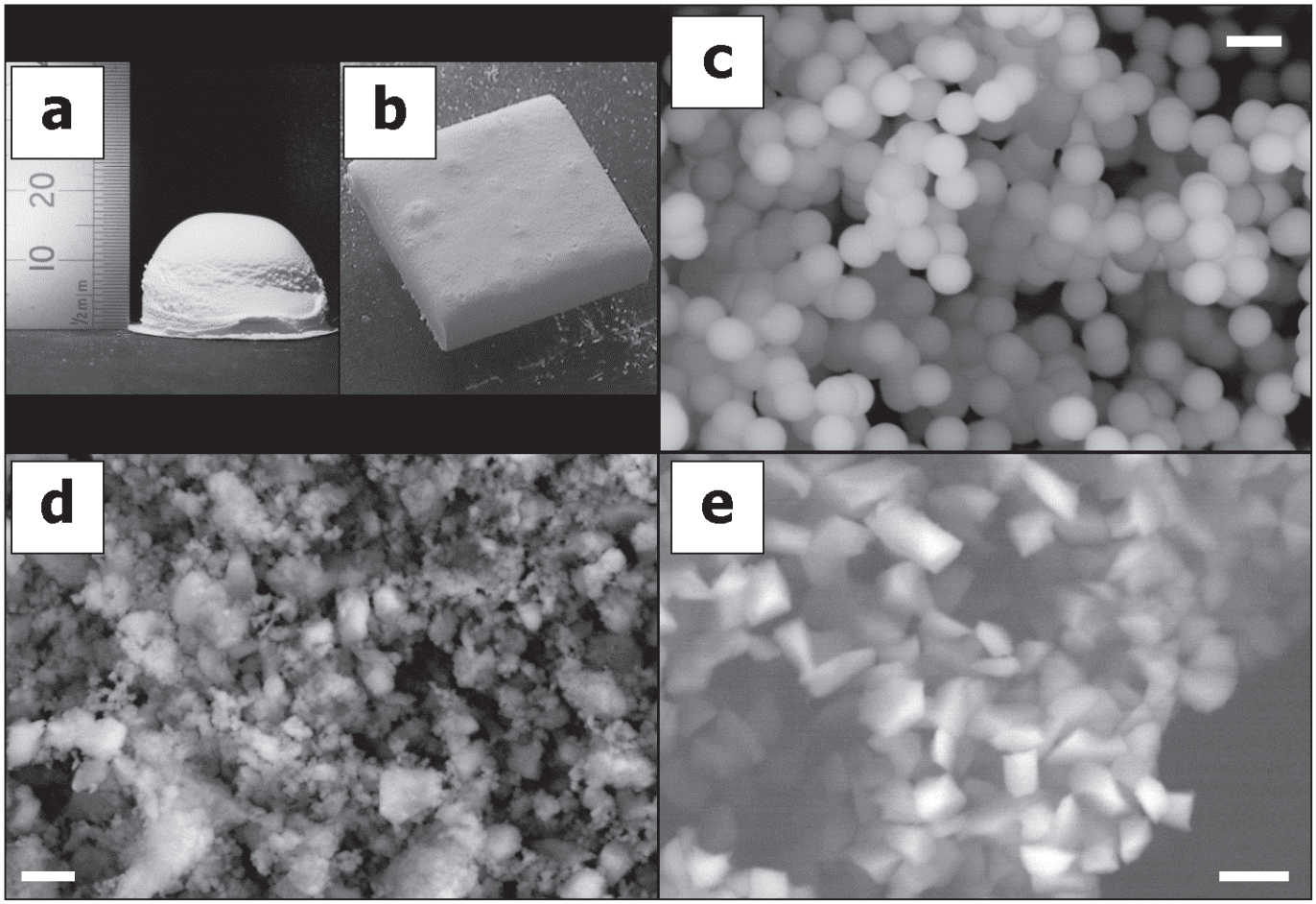


FIG. 2.—(*a*) Photograph of a dust aggregate consisting of spherical monodisperse $SiO_2$ grains. The diameter of the sample is 25 mm. (*b*) A cut section of a dust sample equivalent to that in (*a*). The size of the rectangular sample is $\sim 10 \times 10$ mm$^2$. (*c*) SEM picture of a dust sample consisting of spherical monodisperse $SiO_2$. (*d*) SEM image of a dust sample consisting of irregular polydisperse $SiO_2$. (*e*) SEM image of a dust sample consisting of irregular diamonds. The scale bars indicate 2 $\mu$m. [*See the electronic edition of the Journal for a color version of this figure.*]

window immediately before their deposition on the filter. It was confirmed that the vast majority of dust particles are single grains. To minimize contamination by non-deagglomerated and rather compact dust aggregates that very rarely escape the cogwheel (about 15% of the original dust sample leaves the cogwheel in form of dust clumps), the apparatus was built such that the individual dust grains are guided downward along a succession of curvatures through which larger agglomerates are unable to follow (see Fig. 1).

Typical sedimentation velocities of micron-sized particles in air at 100 Pa pressure are a few cm s$^{-1}$, sufficiently smaller than the gas flow velocity of $\sim 0.5$ m s$^{-1}$ so that $v_{\rm imp} < \min(v_{\rm stick}, v_{\rm roll})$. Due to the mechanical deagglomeration process, the dust grains are charged with up to $\sim 100$–$1000$ elementary charges per monomer (Poppe et al. 1997). However, this charging has no effect on the formation of the dust aggregates (by, e.g., a built-up of strong electrical fields) due to a rapid discharging of the dust on the filter substrate by residual electrical surface conductivity. We measured the electrical resistance of the dust samples and found values in the range $10^8$–$10^{11}$ $\Omega$. With a simple plate capacitor model, we get a capacity of $\sim 1$ pF for our samples so that a discharge timescale of $10^{-3}$–$10^{-1}$ s is expected. This time is much shorter than the formation time of the dust sample ($10^3$–$10^4$ s) so that charge-induced effects are negligible.

A typical example of a dust aggregate is shown in Figure 2*a*. For the determination of the packing density, we cut the dust aggregate by means of a razor blade into quasi-parallelepipeds whose volumes $V$ we could easily determine by high-resolution imaging (Fig. 2*b*). The masses $m$ of these dusty bodies were measured with precision scales (resolution $10^{-5}$ g). The mass density of the sample is then $\rho = m/V$, and the packing densities $\phi = \rho/\rho_0$ can be directly determined.

We determined the compressive strengths of the dust aggregates by compressing cylindrical dust aggregates uniaxially, and we simultaneously measured the thickness of the dust sample, its cross section perpendicular to the applied force, and the compressive force applied. As a result, we got force-compression curves which we converted into relations between pressure and packing density. Uniaxial compression is intended to simulate the compressive effect of impacts, during which the compressed aggregate material is able to flow perpendicular to the impact direction.

For the determination of the tensile strengths of the macroscopic dust agglomerates, we glued two parallel surfaces of the dust samples to very thin glass substrates by means of a nonwetting two-component resin. After the resin had solidified, the samples were inserted into an apparatus that encompassed a micrometer stage with which the thickness of the dust samples could

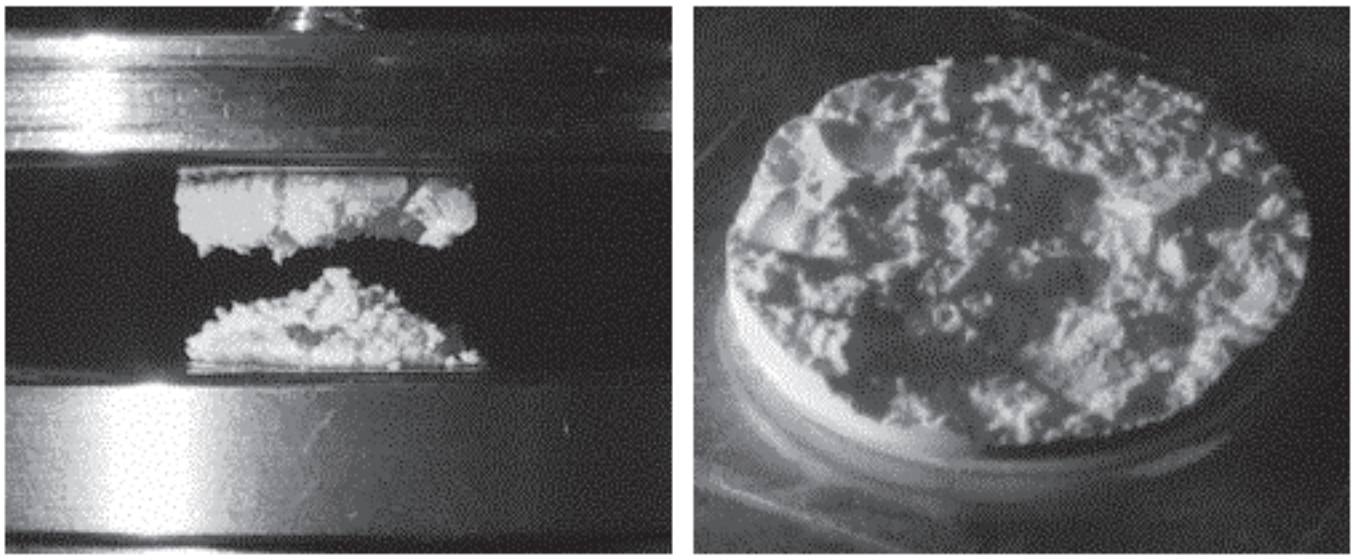

FIG. 3.—Photographs of dust samples after breakage in the tensile-strength experiments. The left image shows the setup with the upper and lower plates to which the dust sample was glued. The right image shows the lower half of a 25 mm dust sample after the tensile-strength experiment. The "valley-and-hill" structure of the new surface is clearly visible. [*See the electronic edition of the Journal for a color version of this figure.*]

be manipulated. For parallization of the samples' surfaces and good contact between the glass substrates and the experimental apparatus, all samples were initially slightly compressed to average values of $\sim 4 \times 10^3$ Pa, corresponding to packing densities of $\phi \approx 0.23$ for the dust samples consisting of monodisperse $SiO_2$ spheres (see § 4.2). The irregular diamond samples were precompressed to average packing densities of $\phi \approx 0.22$, and the irregular $SiO_2$ samples had precompression packing densities of $\phi \approx 0.13$. For the determination of the tensile strengths, the samples were then steadily torn apart. Simultaneous to the induced motion, the force acting on the dust samples was measured. Similar to the measurements of the compressive strengths, we measured the tensile force as a function of linear expansion of the low-density dust samples up to the point of failure at which the samples broke (see Fig. 3). We define this value as the tensile strength of the samples.

## 4. EXPERIMENTAL RESULTS

### 4.1. *Initial Packing Densities*

The dust aggregates formed according to the procedures described in § 3.2 have diameters of 25 mm and are 5–15 mm thick. The samples are homogeneous and have no macroscopic voids throughout their volumes, as shown by the various cuts that were applied. The surfaces of the protoplanetesimal dust analogs are generally very smooth with surface asperities of ~10–30 monomer diameters, in agreement with numerical simulations (J. Blum & T. Kozasa 2006, unpublished data).

The mass densities of our experimental protoplanetesimal dust analogs with spherical $SiO_2$ grains of 0.76 $\mu$m radius fall in the range $(300 \pm 20)$ kg m$^{-3}$. This gives a packing density of $\phi_0 = 0.15 \pm 0.01$. These values are in excellent agreement with the theoretical calculations presented in § 2. The corresponding packing densities of the dust samples consisting of the irregular diamond and $SiO_2$ grains are $\phi_0 = 0.11 \pm 0.02$ and $0.07 \pm 0.03$ (see Table 2).

### 4.2. *Packing Densities under Uniaxial Compressions*

We determined the compression behavior of the dust aggregates using the experimental method described above. The relation between pressure and packing density is presented as a solid black line in Figure 4 for the three different dust samples. The gray lines are the standard deviations derived from multiple measurements of equivalent dust samples. One can distinguish three different zones in the compression curve:

1. As we have seen above, the dust aggregates have packing densities of $\phi_0$ before compression. Below a lower threshold pressure of $p_l$, the packing densities remain constant. Thus, the dust aggregates are mechanically stable against pressures of less than $p_l$. This means that in the laboratory (for static accelerations of $g \approx 10$ m s$^{-2}$) dust aggregates consisting of monodisperse $SiO_2$, for which $p_l \approx 500$ Pa, are stable against gravitational compaction as long as their thickness does not exceed 16 cm.
2. Between $p_l$ and an upper pressure threshold $p_u$, the packing density increases steadily from $\phi_0$ to $\phi_{\max}$.
3. For pressures exceeding $p_u$, the packing density remains constant at a value of $\phi_{\max}$.

The values for $p_l$, $p_u$, $\phi_0$, and $\phi_{\max}$ are summarized in Table 2. The errors of $\phi_0$ for the spherical $SiO_2$ grains in Figure 4 are higher than those given in Table 2. This is due to the fact that $\phi_0$ in Table 2 was determined for a higher number of samples than was used in the compression experiments and due to a direct measurement of the sample volumes.

It must be remarked that the maximum packing densities for all dust samples are far below the theoretical maximum for the packing density for random package of uniform spheres of $\phi = 0.635 \pm 0.005$ (Onoda & Liniger 1990). We could only reach

TABLE 2

MINIMUM AND MAXIMUM PACKING DENSITIES AND LOWER AND UPPER TRANSITION PRESSURES FOR DUST SAMPLES CONSISTING OF SPHERICAL $SiO_2$ PARTICLES, IRREGULAR DIAMONDS, AND IRREGULAR $SiO_2$ GRAINS

| Dust Sample | $\phi_0$ | $\phi_{\max}$ | $p_l$ (Pa) | $p_u$ (Pa) |
|---|---|---|---|---|
| Spherical $SiO_2$ | $0.15 \pm 0.01$ | $0.33 \pm 0.02$ | $\sim 5 \times 10^2$ | $\sim 1 \times 10^5$ |
| Irregular diamond | $0.11 \pm 0.02$ | $0.32 \pm 0.01$ | $\sim 2 \times 10^2$ | $\sim 2 \times 10^5$ |
| Irregular $SiO_2$ | $0.07 \pm 0.03$ | $0.20 \pm 0.01$ | $\sim 2 \times 10^2$ | $\sim 5 \times 10^5$ |

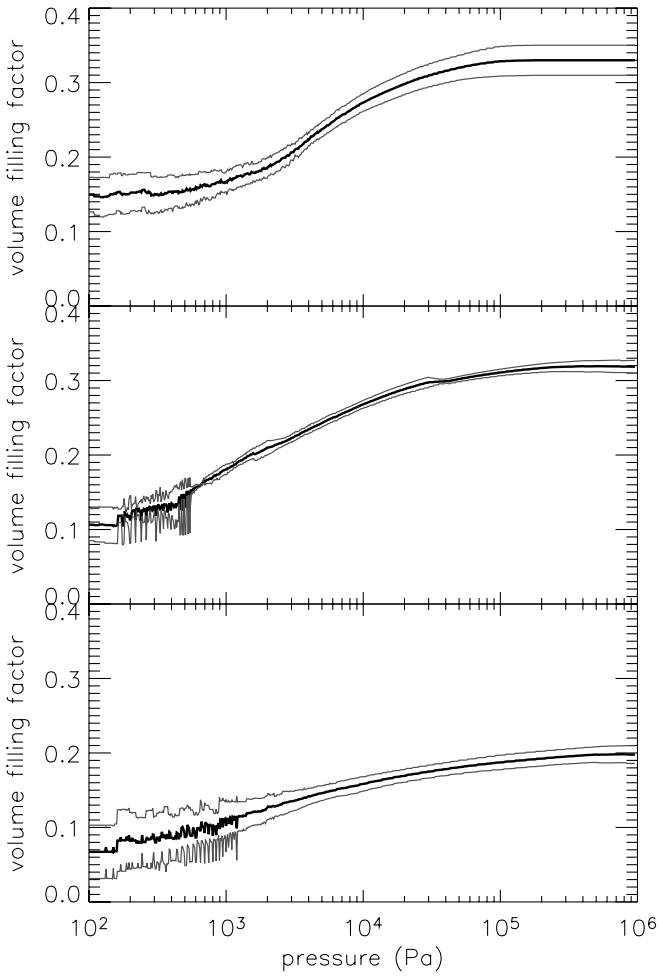


FIG. 4.—Normalized packing density as a function of pressure for dust aggregates consisting of spherical $SiO_2$ grains of 0.76 $\mu$m radius (*top*), for dust samples consisting of irregular diamonds (*center*), and for dust samples consisting of irregular polydisperse $SiO_2$ (*bottom*). The solid black lines denote the mean compression behavior of several dust samples; the gray lines above and below mark the standard deviation of the individual measurements from the mean values.

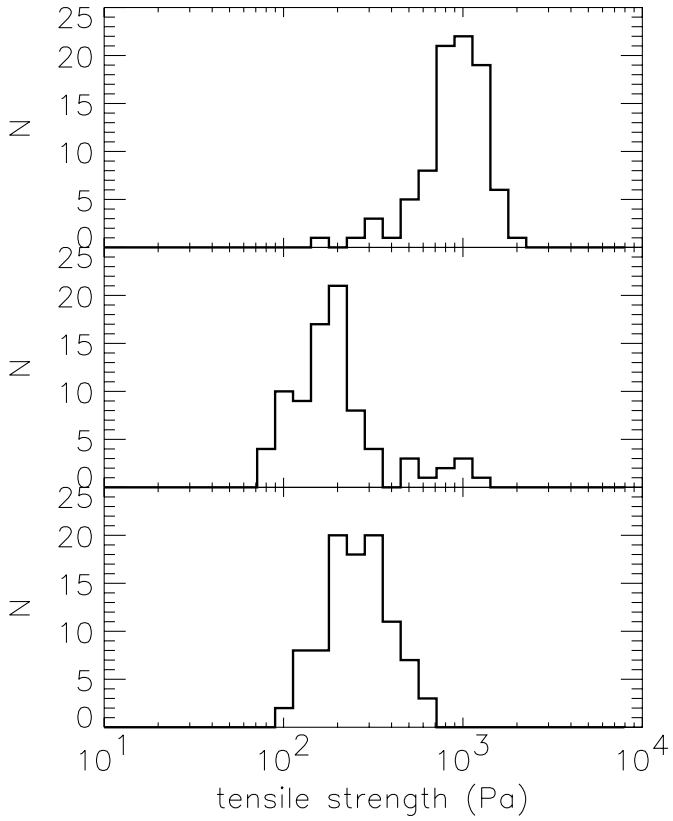


FIG. 5.—Histograms of the measurements of tensile strengths. Shown are the number of experiments per logarithmic tensile strength interval of 0.1 for dust samples consisting of monodisperse, spherical $SiO_2$ grains of $s_0 = 0.75$ $\mu$m diameter (*top*), dust samples consisting of quasi-monodisperse, irregular diamond grains (*center*), and dust samples consisting of polydisperse, irregular $SiO_2$ grains (*bottom*).

values closer to this theoretical limit when we applied *omnidirectional* pressure to the dust samples. Obviously, plastic yield of the agglomerate perpendicular to the applied force prevents a compaction to more than $\phi \sim 0.33$ in uniaxial compression experiments. This view is supported by the observation that the cross section of the dust samples increased steadily above a pressure of $\sim$500 Pa (see Fig. 3 in Blum & Schräpler 2004).

### 4.3. *Tensile Strengths*

In contrast to compression, the dust samples were only weakly resistant to tensile forces. A forced expansion of the samples of a few microns always resulted in the break up of the samples. Due to the preexperimental treatment discussed in § 3, the dust samples consisting of monodisperse $SiO_2$ spheres had average packing densities of $\phi = 0.23$ before disruption.

In Figure 3, two dust samples after breakup are shown. Typically, the samples were disrupted in a "valley-and-hill" fashion, as can be seen in Figure 3. We performed roughly 100 tensile-strength measurements for each of the three types of low-density dust sample types described above. It turned out that the point of disruption, which we identify as the tensile strength of the dust samples, was well defined for each type of dust sample. In Figure 5, the histograms of the tensile-strength measurements for the three dust samples are shown. It can be clearly seen that the distribution of tensile strengths is bell shaped. The average tensile strengths are $Y = 1100$ Pa for monodisperse, spherical $SiO_2$ with $\phi = 0.23$, $Y = 200$ Pa for quasi-monodisperse, irregular diamond with $\phi = 0.22$, and $Y = 300$ Pa for polydisperse, irregular $SiO_2$ with $\phi = 0.13$. The FWHM of the distribution curves is typically a factor of 2–3.

In addition to the low-density dust samples, we also measured the tensile strengths of compacted samples of monodisperse and irregular $SiO_2$ grains. These samples were produced by omnidirectional compression in a standard tablet manufacturing unit. This device did not show the actual compression applied to the samples, so that the repeatability of the sample preparation could only be achieved by counting the number of strokes applied to the manual hydraulic system. We prepared two different sample types for the spherical $SiO_2$ grains and one for the irregular $SiO_2$ particles. The average packing densities of these samples were $\phi = 0.41$ and 0.66 for the spherical $SiO_2$ grains, and $\phi = 0.44$ for the irregular $SiO_2$ grains. It turned out to be impossible to produce dust samples with higher packing densities than $\phi = 0.66$ without breaking up the monomer grains. This maximum packing density is very close to the RCP value of $\phi = 0.635$ (see above).

For the determination of the tensile strengths, the compressed samples were treated the same way as the low-density samples. A large number of single measurements were performed, and the distribution of individual tensile strengths were very similar in shape to the ones demonstrated in Figure 5. The average values for the tensile strengths of the compressed samples were

$Y = 2400$ Pa ($\phi = 0.41$), and $Y = 6300$ Pa ($\phi = 0.66$) for the spherical, monodisperse $SiO_2$ grains. For the irregular, polydisperse $SiO_2$ samples we found $Y = 2300$ Pa for $\phi = 0.44$. Thus, the tensile strengths of the compressed samples is still much smaller than that of solid materials and exceeds those of the low-density dust samples only by a factor of a few.

## 5. SYNTHESIS: PACKING DENSITIES AND TENSILE STRENGTHS OF PROTOPLANETESIMAL MATTER

With our new experimental methods, we are able to produce macroscopic dust agglomerates with very low packing densities. A comparison between the packing densities of the dust aggregates consisting of monodisperse spherical particles with numerical simulations of ballistic hit-and-stick deposition of single spherical grains shows excellent agreement. Thus, our dust samples are potentially well suited to simulate protoplanetesimal matter. As there are no models of the packing densities of dust agglomerates consisting of irregular and/or polydisperse monomer grains available, our experiments can help to reveal the internal structures of realistic protoplanetesimals. The unprocessed dust samples consisting of monodisperse spherical grains have packing densities of $\phi = 0.15$, and the packing densities of uncompacted dust aggregates decrease considerably when irregular monomer grains are used and even more in the case of an additional polydispersity of the monomers. For protoplanetesimal matter this means that the mass densities of macroscopic bodies in the solar nebula depend on the size distribution and shape of the constituent grains.

However, the basic structures of the experimental dust samples do not immediately match those in the solar nebula. Mutual collisions among protoplanetesimals lead to a compaction of the colliding bodies. Models for the collision velocities of macroscopic bodies in the solar nebula show that the mean collision velocities increase with increasing agglomerate size. At the onset of fragmentation, the dust agglomerates have typical diameters of 5 cm, and the mutual collision velocities are typically 1 m s$^{-1}$ (Weidenschilling & Cuzzi 1993; Blum 2004). Such collision velocities lead to dynamical impact pressures of $p_{\rm dyn} \approx \frac{1}{4}\rho v_{\rm imp}^2$ (see § 2). Assuming a packing density of $\phi = 0.15$ and a mean mass density of the material of $\rho_0 = 3 \times 10^3$ kg m$^{-3}$, such collisions will lead to impact pressures of $p_{\rm dyn} \approx 1 \times 10^2$ Pa $\lesssim p_l$. A comparison with the data in Figure 4 shows that at these low pressures, the matter will not be heavily compacted. However, peak dynamic pressures at first contact might exceed $p_l$, so that some minor compaction will result. Thus, we expect centimeter- to decimeter-sized protoplanetary matter to have packing densities $\phi \lesssim 0.15$. The maximum collision velocities are reached when the largest dust agglomerates in the ensemble have sizes of about 1 m. Then, their radial drift velocity will be of the order of 50 m s$^{-1}$ (Weidenschilling & Cuzzi 1993). Thus, the dynamical impact pressure increases to $p_{\rm dyn} \sim 10^6$ Pa $\gtrsim p_u$ (see Table 2). The data in Figure 4 show that these pressures will lead to a considerable compaction of the colliding bodies. For the parameter range investigated in this work, this means that the packing densities of meter-sized protoplanetesimal bodies should fall into the range $\phi = 0.20$–$0.33$. As the mean collision velocity of protoplanetesimal bodies of sizes >1 m do not change considerably, all later unaltered bodies $\gtrsim 1$ m in size should have similar packing densities.

## 6. THE PACKING DENSITIES AND TENSILE STRENGTHS OF PRIMITIVE SOLAR SYSTEM BODIES

Let us now try to compare our experimental findings with the data on packing densities and tensile strengths of the most primitive bodies in the solar system, for which the least alteration over their lifetimes is expected.

### 6.1. *Comets*

Comets are the most primitive bodies currently found in the solar system, which is revealed by their compositional similarities with the interstellar medium in terms of silicates, organic substances, and frozen volatiles (see, e.g., Ehrenfreund et al. 2004). Generally having radii $\lesssim 5$ km (e.g., Fernández et al. 1999; Weissman & Lowry 2003), comets are suitable candidates for the perhaps most interesting class of primordial planetesimals, those that are too small to have been affected by gravitational compression (see eq. [2]), and which thereby carry important clues regarding their agglomeration formation history in their very structure.

However, it is still unknown to what extent cometary nuclei have evolved since the time of solar system formation, i.e., it is not certain that present-day comets indeed are unmodified leftover planetesimals. Impact compaction, catastrophic collisions, and thermal alteration are the major envisioned evolutionary agents. Oort Cloud comets may have been collisionally evolved prior to ejection from the planetary region (Stern & Weissman 2001), and Jupiter-family comets (JFCs), which are believed to originate (see, e.g., Levison & Duncan 1997) from the Edgeworth-Kuiper Belt (EKB), are also likely to have been exposed to impacts. For example, it has been estimated that $\sim 1$ km bodies in the EKB experience 90–300 impacts by bodies larger than 4 m in 3.5 Gyr. In fact, it has been claimed that many JFCs actually are collisional fragments (Stern 1995; Farinella & Davis 1996; Durda & Stern 2000), since the $\lesssim 70$ km tail of the EKB size distribution appears collisionally relaxed (Bernstein et al. 2004). In addition to sublimation-induced alteration due to solar illumination, radiogenic core melting due to $^{26}$Al decay may have led to substantial thermal processing (Prialnik et al. 1987).

Should any of these mechanisms have been important in the past, a direct comparison between comets and primordial planetesimals may be far fetched. With this reservation in mind, we here compare estimated nucleus bulk densities of cometary nuclei, with a plausible density range for compacted cometary material, to arrive at estimates on packing density for these bodies.

The perhaps most accurate estimate of a cometary bulk density to date was obtained recently for comet 9P/Tempel 1, by the NASA *Deep Impact* mission, $\rho_{\rm bulk} = 400 \pm 300$ kg m$^{-3}$ (Richardson & Melosh 2006). Using nongravitational force modeling to estimate the density for the same comet, Davidsson et al. (2006) obtained a very similar value, $\rho_{\rm bulk} = 450 \pm 250$ kg m$^{-3}$. In fact, nongravitational force modeling, which takes into account the momentum transfer of sublimated/condensed gas and ejected dust from a cometary nucleus as well as thermal reradiation from the cometary surface, is one of the most popular methods to estimate comet nucleus densities. The apparition of Comet 1P/Halley in 1986 led to a number of such estimates, clustering around $\rho_{\rm bulk} = 500$–$700$ kg m$^{-3}$ (Rickman 1986, 1989; Sagdeev et al. 1988; Peale 1989; Skorov & Rickman 1999). Furthermore, Rickman et al. (1987) estimated a typical density of $\rho_{\rm bulk} \lesssim 500$ kg m$^{-3}$ for a sample of 17 JFCs. In recent years, nongravitational force modeling has resulted in bulk density estimates for a number of comets, which generally are lower, or much lower, than 1000 kg m$^{-3}$ (see Table 3).

Other techniques for estimating cometary bulk densities include the utilization of tidal disruption, rotational stability, and radar observations. Investigations of the tidally split comet D/1993 F1 Shoemaker-Levy 9 and its fragments that impacted Jupiter in 1994 yielded estimates in the range $250 \lesssim \rho_{\rm bulk} \lesssim 700$ kg m$^{-3}$

TABLE 3
COMETARY DENSITIES

| Density (kg m$^{-3}$) | Comment | Comet | Method | Reference |
|---|---|---|---|---|
| 500−1200 | Lower value preferred | 1P/Halley | NGF | 1, 2, 3 |
| 600(+900/−600) | ... | 1P/Halley | NGF | 4 |
| 700(+4200/−670) | ... | 1P/Halley | NGF | 5 |
| $\lesssim$500 | ... | 17 JFCs | NGF | 6 |
| 490(+340/−200) | ... | 19P/Borrelly | NGF | 7 |
| 180−300 | ... | 19P/Borrelly | NGF | 8 |
| 100−370 | Preferred range | 67P/Churyumov-Gerasimenko | NGF | 9 |
| $\lesssim$600 | ... | 67P/Churyumov-Gerasimenko | NGF | 9 |
| 220−330 | ... | 67P/Churyumov-Gerasimenko | NGF | 10 |
| $\lesssim$600–800 | ... | 81P/Wild 2 | NGF | 11 |
| 450 $\pm$ 250 | ... | 9P/Tempel 1 | NGF | 12 |
| 400 $\pm$ 300 | ... | 9P/Tempel 1 | BED | 13 |
| 600 $\pm$ 100 | Nucleus not rotating | D/1993 F1 Shoemaker-Levy 9 | TD | 14 |
| $\lesssim$1000 | 9 hr period assumed | D/1993 F1 Shoemaker-Levy 9 | TD | 14 |
| 500−600 | ... | D/1993 F1 Shoemaker-Levy 9 | TD | 15 |
| 250 | ... | D/1993 F1 Shoemaker-Levy 9 | JI | 16 |
| $\gtrsim$440 | If strengthless | 6P/d'Arrest | ROT | 17 |
| $\gtrsim$250 | If strengthless | 10P/Tempel 2 | ROT | 17 |
| $\gtrsim$530 | If strengthless | 31P/Schwassmann-Wachmann 2 | ROT | 17 |
| $\gtrsim$350 | If strengthless | 46P/Wirtanen | ROT | 17 |
| $\gtrsim$370 | If strengthless | 95P/Chiron | ROT | 17 |
| $\gtrsim$340 | If strengthless | 107P/Wilson-Harrington | ROT | 17 |
| $\gtrsim$1300 | If strengthless | 133P/Elst-Pizarro | ROT | 18 |
| $\gtrsim$100 | If $Y \gtrsim 200$ Pa | 133P/Elst-Pizarro | ROT | 18 |
| $\gtrsim$200 | If strengthless | C/1991 L3 Levy | ROT | 17 |
| 500−900 | Near-surface layer | C/1983 H1 IRAS-Araki-Alcock | RAD | 19, 20 |
| 500−1000 | Near-surface layer | 2P/Encke | RAD | 20, 21 |
| 700−1300 | Near-surface layer | 26P/Grigg-Skjellerup | RAD | 20, 18 |
| 700−1300 | Near-surface layer | C/1983 J1 Sugano-Saigusa-Fujikawa | RAD | 20, 18 |
| 200−400 | Near-surface layer | C/1996 B2 Hyakutake | RAD | 20, 18 |
| 300−800 | ... | C/1996 B2 Hyakutake | NF | 22 |

NOTES.—For details, refer to text. The methods used for bulk density estimates are nongravitational force modeling (NGF), ballistic ejecta dynamics (BED), tidal disruption modeling (TD), Jupiter impact (JI), stability against rotational breakup (ROT), radar observations (RAD), and nucleus fragmentation (NF).

REFERENCES.—(1) Rickman 1986; (2) Rickman 1989; (3) Skorov & Rickman 1999; (4) Sagdeev et al. 1988; (5) Peale 1989; (6) Rickman et al. 1987; (7) Farnham & Cochran 2002; (8) Davidsson & Gutiérrez 2004; (9) Davidsson & Gutiérrez 2005; (10) Kossacki & Szutowicz 2006; (11) Davidsson & Gutiérrez 2006; (12) Davidsson et al. 2006; (13) Richardson & Melosh 2006; (14) Asphaug & Benz 1996; (15) Solem 1995; (16) Crawford 1997; (17) Davidsson 2001; (18) Davidsson 2006; (19) Harmon et al. 1989; (20) Harmon et al. 1999; (21) Harmon & Nolan 2005; (22) Desvoivres et al. 2000.

(Solem 1995; Asphaug & Benz 1996; Crawford 1997). Stability against disruption due to rotation yields a lower limit on the bulk density only, but most objects investigated so far do not appear to require a bulk density in excess of $\rho_{\rm bulk} \approx 600$ kg m$^{-3}$ even if they are considered totally strengthless (Davidsson 2001; Lowry & Weissman 2003; Toth & Lisse 2006). Radio observations only probe the uppermost few meters of cometary material, and may not be representative of the bulk density of the entire nucleus. In any case, such densities are generally found to be below 1000 kg m$^{-3}$ (Harmon et al. 1989, 1999).

Taking these estimates together (see Table 3), it appears reasonable that the bulk densities of most comets fall inside the range $\rho_{\rm bulk} = 600 \pm 400$ kg m$^{-3}$. We may also estimate a reasonable density for compacted cometary material as $1400 \lesssim \rho_{\rm comp} \lesssim 1700$ kg m$^{-3}$, by applying the mass fractions of silicates (0.26), organic refractories (0.23), volatiles (0.42), and carbonaceous particles (0.09) suggested by Greenberg (1998) and assuming solid densities of these components as $\{\rho_{\rm sil},\ \rho_{\rm org},\ \rho_{\rm vol},\ \rho_{\rm car}\} = \{2700–3500,\ 1800,\ 930–1200,\ 2000\}$ kg m$^{-3}$. This yields a likely packing density of cometary nuclei of $\phi = 0.4 \pm 0.3$. Thus, the lower limit on the packing density coincides with that for PCA or RBD agglomerates, while the upper limit coincides with that for RCP structures. The most likely value, $\phi \approx 0.4$, is somewhat higher than the expected range for protoplanetesimals obtained in the present paper ($0.20 \lesssim \phi \lesssim 0.33$), perhaps indicating that cometary nuclei have been mildly compressed since the time of formation, although nothing certain can be said due to the large error bars. The bulk densities of cometary nuclei are discussed more thoroughly by Weissman et al. (2004) and Davidsson (2006).

Unfortunately, data on cometary tensile strengths are very scarce and in most cases yield lower limits (see Table 4 and Davidsson 2001). Therefore, we will not discuss cometary tensile strengths in depth but only state that current estimates are not in disagreement with our laboratory data.

### 6.2. *Packing Densities and Tensile Strengths of Primitive Meteorites*

Chondritic meteorites are undifferentiated materials that comprise carbonaceous, ordinary, and enstatite classes, which are subdivided into 12 groups (Brearley & Jones 1998; Hutchison 2004). All chondrites are chemically primitive in the sense that the ratios of their major, nonvolatile elements (Fe, Si, Mg, Al, Ca, etc.) are close to those observed in the Sun. However, we will

TABLE 4
COMETARY AND METEOROID TENSILE STRENGTHS

| Tensile Strength (Pa) | Comet/Meteoroid Source | Reference |
|---|---|---|
| | Comet | |
| $10000 > 100-1000$ | Sun-grazing comets | 1 |
| $500 \pm 450$ | 46P/Wirtanen | 2 |
| >3–6 | 6P/d'Arrest | 3 |
| >47 | Levy 1991 XI | 3 |
| >2 | 28P/Neujmin I | 3 |
| >5 | 29P/Schwassmann-Wachmann 1 | 3 |
| >13–53 | 29P/Schwassmann-Wachmann 2 | 3 |
| >6–9 | 10P/Tempel 2 | 3 |
| >4–7 | 107P/Wilson-Harrington | 3 |
| >1 | 46P/Wirtanen | 3 |
| >7700–46000 | 95P/Chiron | 3 |
| >20–400 | C/1996 B2 Huyakutake | 4 |
| | Meteoroid Source | |
| $34000 \pm 7000$ | 2P/Encke (Taurids) | 5 |
| $6000 \pm 300$ | 7P/Pons-Winnecke | 5 |
| $400 \pm 10$ | 21P/Giacobini-Zinner | 5 |
| $22000 \pm 2000$ | 45P/Honda-Mrkos-Pajdusakova (Alpha Capricornids) | 5 |
| $6000 \pm 3000$ | 55P/Tempel-Tuttle (Leonids) | 5 |
| $12000 \pm 3000$ | 109P/Swift-Tuttle (Perseids) | 5 |

REFERENCES.—(1) Klinger et al. 1989; (2) Möhlmann 1996; (3) Davidsson 2001; (4) Lisse et al. 1999; (5) Trigo-Rodríguez & Llorca 2006.

discuss in special detail the carbonaceous chondrite (CC) class. Inside the CCs, several groups (mainly CM, CO, and CRs) exhibit volatile-rich contents located in the fine dust that is cementing these rocks with typical grain sizes of 1 $\mu$m or less. In fact, the different chondrite classes are basically conglomerates of fine dust (a mixture of silicates, oxides, metal, sulfides, and organic constituents), round-shaped spherules called chondrules, and refractory or mafic inclusions (Brearley & Jones 1998). We also know that they are primitive because they contain interstellar grains that survived processing in the solar nebula and that were incorporated to these rocks during accretion (Anders & Zinner 1993). Consequently, these rocks can provide us with insights into the early processes of accretion in the inner solar nebula. However, we should remark here that these meteorites are not in a pristine stage and have experienced parent-body processing to different degrees after accretion (Zolensky & McSween 1988; Brearley & Jones 1998). Consequently, we should take these processes into account in order to compare our laboratory simulation results with the physical properties of these primitive meteorites.

The main processes that occurred after accretion of CCs are aqueous alteration, brecciation, and shock metamorphism. All these processes altered the initial structure and the physical properties of chondritic meteorites that consequently evolved toward higher degrees of compaction. We have already discussed how porous the primitive rocks formed during accretion should be, but we should remark that those rocks have gone through 4.5 Gyr of processing since their formation. A fascinating question is: whether primary accretionary rocks (PARs) are able to survive such a long period without substantial processing. Metzler et al. (1992) coined the PAR term in order to describe very primitive (essentially unaltered) CM chondrites. We use the same terminology in a general sense (to describe the first rocks that evolved to the present chondrites) although we disagree with Metzler's interpretation. Basically, Metzler et al. (1992) described the presence of fine-grained dust mantles around chondrules in CM chondrites and interpreted them as fine-dust material sticking to the chondrules, which have been preserved from the nebular accretionary stage. However, Trigo-Rodríguez et al. (2006) examined nine CM chondrites and concluded that these mantles can be produced by impact-induced shear of a porous precursor that later on suffered extensive aqueous alteration. These authors also noted that aqueous alteration products rich in Fe appear very bright in backscattered electron (BSE) images of the matrix of CM chondrites, giving arguments that these hydrous phases grew preferentially in the empty spaces of the matrix, participating in the progressive compaction of these rocks.

Thermal metamorphism was not very severe in CM and CI chondrites, as is indicated by the peak temperature of 50°C for CMs, and <150°C for CIs derived by Zolensky et al. (1993). Other CCs groups (such as, COs) were thermally metamorphosed at temperatures up to 500°C and beyond, followed by cooling and aqueous alteration. The different degrees of metamorphism experienced by the CCs groups determined the amount of volatiles, aqueous alteration, and compaction that are observed. It is thus very likely that processing of the CC's precursor materials transformed the PARs into very different rocks that, even in the less-altered cases (primitive CCs groups), are exhibiting very different bulk densities and packing densities than their precursors. It is important to remark that the picture is more complicated by the fact that the meteorites that are in our meteorite collections are probably biased toward the toughest samples, since only those more robust materials are able to survive the tensile stresses during violent atmospheric interaction. It is well known that low-strength meteoroids are fragmented to fine dust in the fireball phase (Ceplecha & McCrosky 1976; Ceplecha et al. 1998) (see also § 6.3).

Recent measurements of asteroid bulk densities suggest that porosities of 30%–50% may be common in rubble-pile asteroids

TABLE 5
MEASURED AND MODELED PACKING DENSITIES AND BULK DENSITIES FOR PRIMITIVE METEORITES

| Meteorite Class | Group | $N_{met}$ | Average Packing Density $\phi$ | Bulk Density (kg m$^{-3}$) |
|---|---|---|---|---|
| Carbonaceous chondrite | CM | 18 | $0.770 \pm 0.075$ | $2120 \pm 260$ |
| Carbonaceous chondrite | CO | 8 | $0.802 \pm 0.041$ | $2950 \pm 110$ |
| Carbonaceous chondrite | CV | 10 | $0.862 \pm 0.091$ | $2950 \pm 260$ |
| Carbonaceous chondrite | CI | 4 | 0.887 | 2110 |
| Carbonaceous chondrite | CR | 3 | $0.936 \pm 0.038$ | 3100 |
| Ordinary chondrite | H | 157 | $0.936 \pm 0.042$ | $3400 \pm 180$ |
| Ordinary chondrite | L | 160 | $0.955 \pm 0.046$ | $3350 \pm 160$ |
| Ordinary chondrite | LL | 39 | $0.921 \pm 0.042$ | $3210 \pm 220$ |
| Enstatite chondrite | EH | 5 | $1.012 \pm 0.025$ | $3720 \pm 20$ |
| Enstatite chondrite | EL | 7 | 0.973 | $3550 \pm 100$ |
| Achondrite | Diogenites | 3 | 0.975 | $3260 \pm 170$ |
| Achondrite | Eucrites | 9 | $0.914 \pm 0.046$ | $2860 \pm 70$ |
| Achondrite | Howardites | 5 | $0.953 \pm 0.005$ | $3020 \pm 190$ |
| Achondrite | Aubrites | 6 | 1.000 | $3120 \pm 150$ |
| Achondrite | Ureilites | 3 | 0.911 | $3050 \pm 220$ |
| Stony-Iron | Pallasites | 5 | $1.000 \pm 0.052$ | $4760 \pm 100$ |
| ... | Mesosiderites | 3 | $0.970 \pm 0.081$ | $4250 \pm 20$ |

NOTES.—Only those meteorite groups with a representative number of measured meteorites ($N_{met} \geq 3$) are included. Data from Britt & Consolmagno 2003.

(Britt et al. 2006). However, we should note that it does not mean that the initial porosity of these bodies has been preserved. The high degrees of porosity is associated with cracks and thus with a rubble-pile structure that is decreasing the bulk density of these bodies. In fact, the fluffy aggregates produced in our experiments exhibit packing densities $\phi < 0.33$ for uniaxial compression and $\phi \approx 0.6$–$0.7$ for maximum omnidirectional compression (see § 4.3). If we compare these values with the packing density data shown in Table 5, it is evident that even the recovered meteorites considered most primitive are much more compact. We consider this clear evidence of extensive secondary (postaccretionary) processing of meteorite parent bodies. Thus, the CCs are compacted samples of the nebula matter that, although preserving valuable chemical and isotopic information on the protoplanetary disk environment, exhibit different packing densities than their precursors materials (those we have called PARs). Consequently, aqueous alteration, metamorphism, and impact processes make it very unlikely to find PARs in the present solar system (much more in the meteorite collections). However, we cannot discard a possible exception that unprocessed comets could continue being representative of the precursor materials (see § 6.1).

In order to demonstrate these arguments and to compare the present physical properties of meteoritic material with our laboratory simulations, we have made a search of tensile strengths in the literature (Table 6), which are orders of magnitudes higher than those of our laboratory samples.

TABLE 6
BULK DENSITY, COMPRESSIONAL STRENGTH ($K$), AND TENSILE STRENGTH ($Y$) DETERMINED IN SOME CHONDRITES

| Meteorite | Class | Density (kg m$^{-3}$) | $K$ ($10^5$ Pa) | $Y$ ($10^5$ Pa) | Reference |
|---|---|---|---|---|---|
| Elenovka | L5 | 3500 | 200 | 20 | 1 |
| Krimka | LL3 | 3250 | 1600 | 220 | 1 |
| Tsarev | L5 | 3430 | 3500 | 470 | 1, 2 |
| Kunshak | L5 | 3540 | 2650 | 490 | 1 |
| Kyushu | L6 | 3900 | 980 | 110 | 1 |
| Pulstusk | H5 | 3560 | 2130 | 310 | 1 |
| Holbrok | L6 | (3350)* | 63 | ... | 2, 3 |
| Covert | H5 | (3400)* | 768 | ... | 2, 3 |
| Ness County | L6 | (3350)* | 844 | ... | 2, 3 |
| Kyushu | L6 | (3350)* | 980 | 110 | 2, 3 |
| Krymka | LL3 | (3210)* | 1600 | 220 | 2, 3 |
| Morland | H6 | (3400)* | 1627 | ... | 2, 3 |
| Pultusk | H5 | (3400)* | 2130 | 310 | 2, 3 |
| Alamogordo | H5 | (3400)* | 2740 | ... | 2, 3 |
| Kimble County | H6 | (3400)* | 3270 | ... | 2, 3 |
| Arapahoe | L5 | (3350)* | 4060 | 440 | 2, 3 |
| La Lande | L5 | (3350)* | 4205 | 616 | 2, 3 |

NOTES.—Data between parenthesis is given for averaged class, taken from Britt & Consolmagno 2003. Asterisk (*) denotes average for the meteorite class.

REFERENCES.—(1) Medvedev et al. 1985; (2) Tsvetkov & Skripnik 1991; (3) Britt & Consolmagno 2003.

### 6.3. *Packing Densities and Cometary Strengths Derived from Meteoroids*

Fragmentation of meteoroids in the atmosphere provides additional clues to the strengths of cometary particles. Trigo-Rodríguez & Llorca (2006) have statistically studied the behavior of centimeter-sized or smaller meteoroids during ablation (see data in Table 4). Cometary meteoroids are predicted to be fluffy and likely similar to interplanetary dust particles (IDPs). Their results clearly show that most of the cometary meteoroids that are reaching the terrestrial atmosphere exhibit tensile strengths of $\lesssim 10$ kPa, in agreement with the values measured for our uncompacted dust samples. These strengths are characteristic of known meteoroid streams (e.g., Perseids or Leonids). However, tougher meteoroids with tensile strengths as high as a few kPa exist, such as these coming from very evolved comets (and even presumable inactive comets) as e.g., P/Encke, which is the parent body of the Taurids. A comparison to the tensile-strength data of our compressed samples shows that evolved comets are potentially collisionally compressed. Interestingly, Trigo-Rodríguez & Llorca (2006) also identified extremely fluffy particles coming from 21P/Giacobini-Zinner that typically break apart at extremely low tensile stresses of $\sim$400 Pa, an indication of the presence of very small grains.

The study of the ablation of fireballs in the atmosphere can provide additional clues on the meteoroids' packing densities. Gustafson & Adolfsson (1997) demonstrated that in favorable cases the bulk density and porosity of meteoroids during atmospheric flight can be estimated. By using the data obtained during ablation of the European Network type IIIb bolide (EN 71177), they estimated a bulk density of 260 kg m$^{-3}$. From this result they obtained the packing factor by calculating the ratio of the density of the compact material of chondritic composition (assumed by Gustafson and Adolfsson 1997 to be $\rho_c = 2400$ kg m$^{-3}$) to the bulk density. They estimated that the meteoroid was $\sim$0.7 kg in mass and had a porosity of $\pi \approx 0.88$. This high value is in full accord with the maximum values of porosity estimated for IDPs (Rietmeijer 1998, 2002, 2005; Flynn 2005).

## 7. TOWARDS A MODEL OF PROTOPLANETARY DUST PROPERTIES: ESTIMATING THE TENSILE STRENGTH OF PROTOPLANETESIMAL MATTER

To understand the microphysics involved in the disintegration process of a large agglomerate, we compare the maximum separation force per unit area, i.e., the tensile strength, and the total energy required for the disruption of the sample to the forces and energies on the monomer-particle level. The number of monomers within a volume of cross-sectional area $A$ and thickness $2s_0$ is given by

$$N = \phi \frac{2As_0}{(4/3)\pi s_0^3} = \phi \frac{3A}{2\pi s_0^2}. \tag{3}$$

To a reasonable approximation, we can set the number of monomer-monomer contacts that are separated during the disintegration process equal to the number of monomers (i.e., each monomer has basically two neighbors) so that we get

$$N_{\rm sep} \approx \phi \frac{3A}{2\pi s_0^2}. \tag{4}$$

The maximum force required to separate the two halves of the sample is then given by

$$F_{\rm max} = N_{\rm sep} F_{\rm stick}, \tag{5}$$

and with Equations (4) and (5) the tensile strength is

$$Y \leq \frac{F_{\rm max}}{A} = \frac{3\phi F_{\rm stick}}{2\pi s_0^2} \approx 11000 \text{ Pa} \tag{6}$$

for $\phi = 0.2$, and the data given in Table 1. However, equation (6) gives only an upper limit to the tensile strength, because not all monomer-monomer contacts break simultaneously. This can be seen by the force-displacement curve shown in Figure 4 of Blum & Schräpler (2004). A lower limit to the tensile strength can be obtained if we consider the total energy required for the disintegration of the sample. For simplicity, we set the total energy required for separation, $W_{\rm sep}$, equal to the product of the measured tensile strength, the typical separation distance $d_{\rm sep}$, and the sample cross section, i.e.,

$$W_{\rm sep} = Y d_{\rm sep} A. \tag{7}$$

From our experiments, the best estimate for the separation distance is $d_{\rm sep} = (10 \pm 5)\ \mu$m. Due to the here neglected rolling and sliding between monomer grains during separation, and the corresponding energy losses, a lower limit to the total separation energy is given by the sum of all monomer-monomer adhesion energies $E_{\rm stick}$ (see Table 1), hence

$$W_{\rm sep} \geq N_{\rm sep} E_{\rm stick} \approx \phi \frac{3A}{2\pi s_0^2} E_{\rm stick}. \tag{8}$$

By inserting equation (8) in equation (7), we get for the tensile strength

$$Y \geq \frac{3\phi E_{\rm stick}}{2\pi s_0^2 d_{\rm sep}} = 36 \text{ Pa}. \tag{9}$$

Comparing the results of our tensile-strength measurements with the estimates given by equations (6) and (9) shows that the measured data of $Y \approx 1000$ Pa fall indeed into the range 36 Pa $\leq Y \leq$ 11000 Pa. It is obvious that for a detailed derivation of the tensile strength of agglomerates all interaction forces, in particular the rolling-friction force, between neighboring monomer particles inside the agglomerate need to be taken into account.

The lower tensile strengths of the dust agglomerates consisting of nonspherical monomer grains can be explained by weaker grain-grain contacts than in the case of spherical grains (where all contacts are equal). Irregular grains consist of plane surfaces, edges, and sharp tips (see Figs. 2*d*–2*e*). Whenever an edge or a tip are involved in a grain-grain contact, the adhesion forces are much weaker than in a contact between two plane surfaces or between two spherical grains with a larger radius of curvature. The likelihood of a contact involving an edge or a tip is much higher than that between two planar surfaces. Thus, we expect agglomerates consisting of irregular dust grains to be weaker than those made of spherical grains, in agreement with our observations (see Fig. 5).

The only two models available in the astrophysical literature for the tensile strength of loosely packed granular matter were published by Greenberg et al. (1995) and Sirono & Greenberg (2000). In their cometary tensile-strength model, Greenberg et al. (1995) assume a homogeneous body with no radial stratification consisting of spherical grains of radius $s_0$. They derive tensile strengths of

$$Y = 6 \times 10^2 \phi\beta \left(\frac{s_0}{0.1\ \mu\text{m}}\right)^{-2} \text{ Pa}. \tag{10}$$

The coefficient $\beta$ describes the number of next neighbors in the macroscopic dust agglomerate. Setting $s_0$ to the typical particle radii in our experiments $s_0 = 0.76$ $\mu$m, $\phi = 0.2$, and $\beta = 3$, a typical value for loosely-packed matter, we get $T = 6$ Pa. This is a few orders of magnitude below our measured values. The model by Sirono & Greenberg (2000) estimates the tensile strength by the cutting of particle chains that form a cubic lattice. For the tensile strength, Sirono & Greenberg (2000) get

$$Y = \frac{F_{\rm stick}}{l^2}, \tag{11}$$

where $F_{\rm stick}$ is the separation force for a single grain-grain contact and $l$ is the length of a chain. As a chain must at least consist of two particles, $l \geq 2s_0$, we get with the data from Table 1, $Y \leq 29000$ Pa. A better estimate on the length of a particle chain can be reached by identifying the separation distance in our tensile-strength experiments, $d_{\rm sep} = (10 \pm 5)$ $\mu$m, with the typical length of a particle chain, i.e., $l = d_{\rm sep}$. With this, we get $Y = (670 \pm 335)$ Pa, which is rather close to our measured value of $Y = 1100$ Pa. Thus, our observations of tensile strengths and the force-displacement behavior in the tensile experiments are consistent with the model by Sirono & Greenberg (2000). However, a model for the length of particle chains in loose dust aggregates does not exist.

As we have seen in § 2, random close packing of spheres leads to a packing density of $\phi = 0.635$ (Onoda & Liniger 1990; Torquato et al. 2000). If we assume that planetesimals and cometesimals are inhomogeneous on a macroscopic scale, i.e., consist of large substructures with *macroscopic* voids in between ("primordial rubble piles"; Weissman 1986), and these substructures themselves consist of smaller entities and voids, then we can easily get to a packing density similar to that found in our laboratory experiments for *homogenous* RBD aggregates and for comets. It is clear that the different possible internal structures of planetesimals/cometesimals reflect their growth history. Due to the existence of macroscopic entities and voids in the alternative model, the fragmentation behavior and possibly also the tensile strength of comets could reveal the nature of their formation. More work on modeling, experiments, and observations on cometary fragmentation is needed before an unambiguous answer to the problem of planetesimal structures can be given.

## 8. CONCLUSION

For protoplanetesimal sizes of $\gtrsim 1$ m, when the mean collision velocities do not change drastically any more (Weidenschilling & Cuzzi 1993), our experimental results suggest that, depending on size distribution and morphology of the constituent dust grains, the packing densities of these protoplanetesimals fall into the range $\phi = 0.20$–$0.33$.

Our measurements of the tensile strengths of low-density dust agglomerates show that the disruption of these bodies happens at values of typically $Y = 1$ kPa. With icy constituent grains, whose interparticle forces should be higher than those of $SiO_2$ by a factor of $\sim$3.5 (Petrenko & Whitworth 1999), we expect for cometesimals tensile strengths of $10^3$–$10^4$ Pa. Thus, packing densities and tensile strengths are in good agreement with measurements at comets and meteoroids (see Tables 3 and 4).

The study of primitive meteorites can provide interesting clues to the postaccretionary physical properties of these rocky aggregates. However, even the less-processed meteorites exhibit clear evidence for parent-body processing, especially impact-induced compaction and aqueous alteration. In order to study these processes and search for analogies in laboratory experiments, it is necessary to get additional data on the strength of primitive meteorites. Currently, reliable strength information is available for a limited number of ordinary chondrites only. Moreover, we encourage future modeling of the evolution of physical properties of minor bodies.

We have shown that the determination of the strength of solar system materials can provide valuable information on the nature, and the complex evolutionary history of minor bodies. However, we are still far from a comprehensive model of the mechanical and collision properties of protoplanetary matter with which reliable predictions about the evolution of protoplanetary bodies can be made. This will be the subject of further studies.

## 9. OUTLOOK

With the new macroscopic dust samples, we now have excellent laboratory analogs for further experimental studies. These studies will first encompass collision experiments to be presented in a forthcoming paper. The next steps will be experiments on the formation of chondrules from high-porosity dust analogs by fast melting, experiments on thermal conductivity, and cometary simulation. The ultimate goal of these studies will be a concise model for the growth and internal structures of protoplanetary bodies of all sizes from decimeter to kilometer. Therefore, collaborative efforts of theorists, modelers, and experimentalists are mandatory.

The laboratory experiments were funded by the German Space Agency (DLR) under contract No. 50 WM 0036 and 50 WM 0336 as part of the ICAPS program.

## REFERENCES

Anders, E., & Zinner, E. 1993, Meteoritics, 28, 490
Asphaug, E., & Benz, W. 1996, Icarus, 121, 225
Bernstein, G. M., Trilling, D. E., Allen, R. L., Brown, M. E., Holman, M., & Malhotra, R. 2004, AJ, 128, 1364
Blum, J. 2004, in ASP Conf. Ser. 309, Astrophysics of Dust, ed. A. N. Witt, G. C. Clayton, & B. T. Draine (San Francisco: ASP), 369
———. 2006, Adv. in Phys., in press
Blum, J., & Münch, M. 1993, Icarus, 106, 151
Blum, J., & Schräpler, R. 2004, Phys. Rev. Lett., 93, 550
Blum, J., & Wurm, G. 2000, Icarus, 143, 138
Blum, J., Wurm, G., Poppe, T., & Heim, L.-O. 1998, Earth Moon Planets, 80, 285
Blum, J., et al. 2000, Phys. Rev. Lett., 85, 2426
Brearley, A., & Jones, R. H. 1998, in Reviews in Mineralogy 36, Planetary Materials, ed. J. J. Papike (Washington: Mineral. Soc. America), 3
Britt, D. T., & Consolmagno, G. J. 2003, Meteoritics Planet. Sci., 38, 1161
Britt, D. T., Consolmagno, G. J., & Merline, W. J. 2006, in Lunar Planet. Sci. 37 (Houston: LPI), Abst. 2214
Ceplecha, Z., Borovička, J., Elford, W. G., Revelle, D. O., Hawkes, R. L., Porubcan, V., & Simek, M. 1998, Space Sci. Rev., 84, 327
Ceplecha, Z., & McCrosky, R. E. 1976, J. Geophys. Res., 81, 6257
Crawford, D. A. 1997, Lunar Planet. Sci., 28, 267
Davidsson, B. J. R. 2001, Icarus, 149, 375
———. 2006, Adv. Geosci., in press
Davidsson, B. J. R., & Gutiérrez, P. J. 2004, Icarus, 168, 392
———. 2005, Icarus, 180, 224
———. 2006, Icarus, in press
Davidsson, B. J. R., Gutiérrez, P. J., & Rickman, R. 2006, Icarus, 180, 224
Desvoivres, E., Klinger, J., Levasseur-Regourd, A. C., & Jones, G. H. 2000, Icarus, 144, 172
Dominik, C., & Tielens, A. G. G. M. 1997, ApJ, 480, 647
Durda, D. D., & Stern, S. A. 2000, Icarus, 145, 220
Ehrenfreund, P., Charnley, S. B., & Wooden, D. H. 2004, in Comets II, ed. M. C. Festou, H. U. Keller, & H. A. Weaver (Tucson: Univ. Arizona Press), 115
Farinella, P., & Davis, D. R. 1996, Science, 273, 938
Farnham, T. L., & Cochran, A. L. 2002, Icarus, 160, 398

Fernández, J. A., Tancredi, G., Rickman, H., & Licandro, J. 1999, A&A, 352, 327
Flynn, G. J. 2005, Earth Moon Planets, 95, 361
Greenberg, J. M. 1998, A&A, 330, 375
Greenberg, J. M., Mizutani, H., & Yamamoto, T. 1995, A&A, 295, L35
Gustafson, B. A. S., & Adolfsson, L. G. 1997, in The Cosmic Dust Connection, ed. J. M. Greenberg (NATO ASI Ser. C, 487; Dordrecht: Kluwer), 349
Harmon, J. K., Campbell, D. B., Hine, A. A., Shapiro, I. I., & Marsden, B. G. 1989, ApJ, 338, 1071
Harmon, J. K., Campbell, D. B., Ostro, S. J., & Nolan, M. C. 1999, Planet. Space Sci., 47, 1409
Harmon, J. K., & Nolan, M. C. 2005, Icarus, 176, 175
Heim, L.-O., Blum, J., Preuss, M., & Butt, H.-J. 1999, Phys. Rev. Lett., 83, 3328
Hutchison, R. 2004, Meteorites (Cambridge: Cambridge Univ. Press)
Klinger, J., Espinasse, S., & Schmidt, B. 1989, in Physics and Mechanics of Cometary Materials (ESA SP-302; Noordwijk: ESA), 197
Kossacki, K. J., & Szutowicz, S. 2006, Planet. Space Sci., 54, 15
Kozasa, T., Blum, J., & Mukai, T. 1992, A&A, 263, 423
Krause, M., & Blum, J. 2004, Phys. Rev. Lett., 93
Levison, H. F., & Duncan, M. J. 1997, Icarus, 127, 13
Lisse, C. M., et al. 1999, Icarus, 140, 189
Lowry, S. C., & Weissman, P. R. 2003, Icarus, 164, 492
Medvedev, R. V., Gorbatsevich, F. I., & Zotkin, I. T. 1985, Meteoritika, 44, 105
Metzler, K., Bischoff, A., & Stöffler, D. 1992, Geochim. Cosmochim. Acta, 56, 2873
Möhlmann, D. 1996, Planet. Space Sci., 44, 541
Onoda, G. Y., & Liniger, E. G. 1990, Phys. Rev. Lett., 64, 2727
Peale, S. J. 1989, Icarus, 82, 36
Petrenko, V. F., & Whitworth, R. W. 1999, Physics of Ice (Oxford: Oxford Univ. Press)
Poppe, T., Blum, J., & Henning, T. 1997, Rev. Sci. Instrum., 68, 2529
———. 2000a, ApJ, 533, 454
———. 2000b, ApJ, 533, 472
Poppe, T., & Schräpler, R. 2005, A&A, 438, 1
Prialnik, D., Bar-Nun, A., & Podolak, M. 1987, ApJ, 319, 993
Richardson, J. E., & Melosh, H. J. 2006, in Lunar Planet. Sci. 37 (Houston: LPI), Abst. 1836
Rickman, H. 1986, in Proc. of Comet Nucleus Sample Return Mission, ed. O. Melita (ESA SP-249; Noordwijk: ESA ), 195
———. 1989, Adv. Space Res., 9, 59
Rickman, H., Kamél, L., Festou, M. C., & Froeschlé, C. 1987, in Proc. Symposium on the Diversity and Similarity of Comets, ed. E. J. Rolfe & B. Battrick (ESA SP-278; Noordwijk: ESA), 471
Rietmeijer, F. J. M. 1998, Reviews in Mineralogy, 36, 2
———. 2002, Chemie der Erde, 62, 1
———. 2005, Earth Moon Planets, 95, 321
Sagdeev, R. Z., Elyasberg, P. E., & Moroz, V. I. 1988, Nature, 331, 240
Sekiya, M., & Takeda, H. 2003, Earth, Planets, Space, 55, 263
Sirono, S.-I. 2004, Icarus, 167, 431
Sirono, S.- I., & Greenberg, J. M. 2000, Icarus, 145, 230
Skorov, Y. V., & Rickman, H. 1999, Planet. Space Sci., 47, 935
Smoluchowski, M. V. 1916, Physik Zeit., 17, 557
Solem, J. C. 1995, A&A, 302, 596
Stern, S. A. 1995, AJ, 110, 856
Stern, S. A., & Weissman, P. R. 2001, Nature, 409, 589
Torquato, S., Truskett, T. M., & Debenedetti, P. G. 2000., Phys. Rev. Lett., 84, 2064
Toth, I., & Lisse, C. M. 2006, Icarus, 181, 162
Trigo-Rodríguez, J. M., & Llorca, J. 2006, MNRAS, 372, 655
Trigo-Rodríguez, J. M., Rubin, A. E., & Wasson, J. T. 2006, Geochim. Cosmochim. Acta, 70, 1271
Tsvetkov, V. I., & Skripnik, A. Ia. 1991, Astron. Vestnik, 25, 364
Watson, P. K., Mizes, H., Castellanos, A., & Pérez, A. 1997, in Powders & Grains 97, ed. R. Behringer & J. T. Jenkins (Rotterdam: A. A. Balkema), 109
Weidenschilling, S. J. 1977, MNRAS, 180, 57
———. 1997, Icarus, 127, 290
Weidenschilling, S. J., & Cuzzi, J. N. 1993, in Protostars and Planets III, ed. E. H. Levy & J. I. Lunine (Tucson: Univ. Arizona Press), 1031
Weissman, P. R. 1986, Nature, 320, 242
Weissman, P. R., Asphaug, E., & Lowry, S. C. 2004, in Comets II, ed. M. C. Festou, H. U. Keller, & H. A. Weaver (Tucson: Univ. Arizona Press), 337
Weissman, P. R., & Lowry, S. C. 2003, in Lunar Planet. Sci. 34 (Houston: LPI), Abst. 2003
Wurm, G., & Blum, J. 1998, Icarus, 132, 125
Wurm, G., Blum, J., & Colwell, J. E. 2001a, Icarus, 151, 318
———. 2001b, Phys. Rev. E, 64, 046301
Wurm, G., Paraskov, G., & Krauss, O. 2004, ApJ, 606, 983
———. 2005, Icarus, 178, 253
Zolensky, M. E., Barret, T., & Browning, L. 1993, Geochim. Cosmochim. Acta, 57, 3123
Zolensky, M. E., & Mc Sween, H. 1988, in Meteorites and the Early Solar System, ed. J. F. Kerridge & M. S. Matthews (Tucson: Univ. Arizona Press), 114